

# A Regularization Approach to Blind Deblurring and Denoising of QR Barcodes

Yves van Gennip\* Prashant Athavale<sup>†</sup> Jérôme Gilles<sup>‡</sup> Rustum Choksi<sup>§</sup>

May 17, 2022

## Abstract

Using only regularization-based methods, we provide an ansatz-free algorithm for blind deblurring of QR bar codes in the presence of noise. The algorithm exploits the fact that QR bar codes are prototypical images for which part of the image is a priori known (finder patterns). The method has four steps: (i) denoising of the entire image via a suitably weighted TV flow; (ii) using a priori knowledge of one of the finder corners to apply a higher-order smooth regularization to estimate the unknown point spread function (PSF) associated with the blurring; (iii) applying an appropriately regularized deconvolution using the PSF of step (ii); (iv) thresholding the output. We assess our methods via the open source bar code reader software *ZBar* [1].

**Ocis codes:** (070.0070) Fourier optics and signal processing; (100.0100) Image processing.

## 1 Introduction

Invented in Japan by the Toyota subsidiary Denso Wave in 1994, QR bar codes (*Quick Response bar codes*) are a type of matrix 2D bar codes ([2, 3, 4]) that was originally created to

track vehicles during the manufacturing process (see Figure 1). Designed to allow its contents to be decoded at high speed, they have now become the most popular type of matrix 2D bar codes and are easily read by most smartphones.

Whereas standard 1D bar codes are designed to be mechanically scanned by a narrow beam of light, a QR bar code is detected as a 2D digital image by a semiconductor image sensor and is then digitally analyzed by a programmed processor ([2, 4]). Key to this detection are a set of required patterns, so-called *finder patterns*, which consist of three fixed squares at the top and bottom left corners of the image, a smaller square near the bottom right corner for alignment and two lines of pixels connecting the two top corners at their bottoms and the two left corners at their right sides. Figure 2 shows gives a schematic of a QR bar code, in particular showing these required squares.

In this article we address blind deblurring of QR bar codes in the presence of noise. This is a problem of considerable interest. While mobile smartphones equipped with a camera are increasingly used for QR bar code reading, limitations of the camera imply that the captured images are always blurry and noisy. There are many sources for camera blurring, for example the relative motion between the camera and bar code, and deblurring is important to optimize the *depth of field*, the distance between the nearest and farthest objects in a part of the scene which appears acceptably sharp in the image ([5]). Thus methods for truly blind deblurring,

\*School of Mathematical Sciences, University of Nottingham

<sup>†</sup>Fields Institute, University of Toronto

<sup>‡</sup>Department of Mathematics & Statistics, San Diego State University

<sup>§</sup>Department of Mathematics and Statistics, McGill University



Figure 1: A QR bar code (used as “Code 1” in the tests described in this paper). Source: Wikipedia [4]

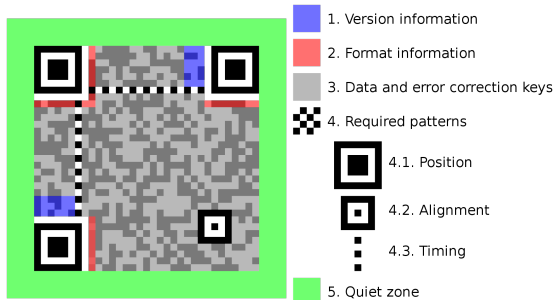


Figure 2: Anatomy of a QR bar code. Best viewed in color. Source: Wikipedia [4]

i.e., ansatz-free with respect to possible point spread functions, are important for the successful use of mobile smartphones ([6, 7, 8, 9, 10]).

### 1.1 Existing Approaches for Blind Deblurring of Bar codes

First off, we note that there are currently a wealth of regularization-based methods for blind deblurring of general images. For a signal  $f$  many attempt to minimize over all  $u$  and point spread functions  $\phi$ ,

$$\mathcal{E}(u, \phi) = \mathcal{F}(u * \phi - f) + \mathcal{R}_1(u) + \mathcal{R}_2(\phi),$$

where  $\mathcal{F}$  denotes a fidelity term and the  $\mathcal{R}_i$  are regularizers, often of TV (total variation) type

(cf. [11, 12, 13, 14, 15, 16, 17, 18, 19]). Recently there is work which uses sparsity-based priors to regularize the images and point spread functions (cf. [20, 21, 22, 23, 24]).

On the other hand, the simple structure of bar codes has lent itself to specific blind deblurring methods, both regularization and non-regularization based. Much work has been done on 1D bar codes (see for example, [25, 5, 26, 27, 28, 29, 30, 31]). 2D matrix and stacked bar codes ([2]) have received less attention (see for example [32, 33, 34]). The paper of Liu et al [34] is the closest to the present work, and proposes an iterative *Increment Constrained Least Squares filter* method for certain 2D matrix bar codes within a Gaussian blurring ansatz. In particular, they use the L-shapes finder pattern of their codes to estimate the standard deviation of the Gaussian PSF, and then restore the image by successively implementing a bi-level constraint.

### 1.2 Our Approach for QR Bar Codes

Our framework for the problem is as follows. Let  $z$  denote the characteristic function of the black area of a QR bar code. A scan of the bar code leads to a measured signal  $f$ , which is a blurry and noisy version of the clean bar code  $z$ . We assume that  $f$  is of the form  $f = N(\phi_b * z)$ , where  $\phi_b$  is the point spread function (PSF) or blurring kernel and  $N$  is a noise operator. Parts of the bar code are assumed known. In particular, we focus on the known top left corner of a QR bar code. Our goal in this paper is to exploit the known information to accurately estimate the unknown PSF  $\phi_b$ , and to complement this with state of the art methods in total variation (TV) based regularizations for deconvolution and denoising. Specifically, we perform the following four steps:

- (i) denoising the signal via a weighted TV flow;
- (ii) estimating the PSF by a higher-order smooth regularization based upon comparison of the known finder pattern in the upper left corner with the denoised signal from

- step (i) in the same corner;
- (iii) applying appropriately regularized deconvolution with the PSF of step (ii);
  - (iv) thresholding the output of step (iii).

We note that, in principle, our method extends to blind deblurring and denoising of images for which a fixed part of the image is *a priori known*. We focus on QR bar codes because

- they present a canonical class of ubiquitous images possessing this property;
- their simple structure of blocks lends itself well to a simple anisotropic TV regularization;
- software is readily available to both generate and *read* QR bar codes. The latter gives rise to a simple and unambiguous way in which to assess our methods: That is, for a blurry and noisy signal  $f$  of a QR bar code which is *unreadable* by a given software, we can test whether or not our deblurred-denoised signal is in fact *readable*. To this end, we create a large dataset of blurry and noisy QR bar codes and perform an evaluation using the open source software *ZBar* [1].

## 2 TV Regularization and Split Bregman Iteration

Since the seminal paper of Rudin-Osher-Fatemi [35], TV (*i.e.*, the  $L^1$  norm of the gradient) based regularization methods have proven to be successful for image denoising and deconvolution. Since that time, several improvements have been explored, such as anisotropic ([36, 37]) and nonlocal ([38]) versions of TV. Let us recall the philosophy of such models by describing the anisotropic TV denoising case.

This method constructs a restored image  $u_0$  from an observed image  $f$  by solving

$$u_0 = \underset{u}{\operatorname{argmin}} \|\nabla u\|_1 + \frac{\mu}{2} \|u - f\|_2^2, \quad (1)$$

where  $\|\nabla u\|_1 = |u_x| + |u_y|$  (here  $u_x, u_y$  are the partial derivatives of  $u$  in the  $x$  and  $y$  directions, respectively). One of the current state of the art methods for the fast numerical computation of TV based regularization schemes is split Bregman iteration ([39, 40, 41]). It consists of splitting the above minimization problem into several problems which are easier to solve by introducing extra variables  $d_x = u_x$  and  $d_y = u_y$  (the subscripts in the new variables do not denote differentiation). Solving for (1) is equivalent to finding  $u_0, d_x, d_y$  which solve the following steps ([39, 40]):

1.  $(u^{k+1}, d_x^{k+1}, d_y^{k+1}) = \operatorname{argmin} \|d_x\|_1 + \|d_y\|_1 + \frac{\mu}{2} \|u - f\|_2^2 + \frac{\lambda}{2} \|d_x - u_x + b_x^k\|_2^2 + \frac{\lambda}{2} \|d_y - u_y + b_y^k\|_2^2$
2.  $b_x^{k+1} = b_x^k + u_x^{k+1} - d_x^{k+1}$
3.  $b_y^{k+1} = b_y^k + u_y^{k+1} - d_y^{k+1}$

Then  $u_0$  will be given by the final  $u^k$ .

The first step can be handled by alternatively fixing two of the variables and then solving for the third one. It is easy to see that if we fix  $d_x$  and  $d_y$  we get an  $L^2 - L^2$  problem which can be efficiently solved by a Gauss-Seidel scheme [40] or in the Fourier domain [41]. Here we take the Fourier approach. The updates  $d_x^{k+1}, d_y^{k+1}$  correspond to the solution of  $L^1 - L^2$  type problems and are given by

$$\begin{aligned} d_x^{k+1} &= \operatorname{shrink}(u_x^{k+1} + b_x^k, 1/\lambda) \\ d_y^{k+1} &= \operatorname{shrink}(u_y^{k+1} + b_y^k, 1/\lambda) \end{aligned}$$

where the operator *shrink* is given by  $\operatorname{shrink}(v, \delta) = \operatorname{sign}(v) \max(0, |v| - \delta)$ .

## 3 The Method

### 3.1 Creating Blurred and Noisy QR Test Codes

We ran our tests on a collection of QR bar codes, some of which are shown in Figure 7. In each case, the clean bar code is denoted by  $z$ . The

*module width* denotes the length of the smallest square of the bar code (the analogue of the  $X$ -dimension in a 1D bar code). In each of the QR codes we used for this paper, for example those in Figure 7, this length consists of 8 pixels. In fact, we can automatically extract this length from the clean corners or the timing lines in the bar codes.

We create blurry and noisy versions of the clean bar code  $z$  as follows. We use MATLAB’s function “fspecial” to create the blurring kernel  $\phi_b$ . In this paper we discuss results using Gaussian blur (a rotationally symmetric Gaussian lowpass filter with prescribed size and standard deviation) and motion blur (a filter which approximates, once convolved with an image, the linear motion of a camera by a prescribed number of pixels, with an angle of thirty degrees in a counterclockwise direction). The convolution is performed using MATLAB’s “imfilter(·, ‘conv’)” function.

In our experiments we apply one of four types of noise operator  $N$  to the blurred bar code  $\phi_b * z$ :

- *additive random noise*, via the addition to each pixel of a pseudorandom number drawn from the standard normal distribution (MATLAB’s function “randn”);
- *Gaussian noise* (with prescribed mean and variance), created by adding the mean value to each pixel and then adding the square root of the variance times a uniformly distributed pseudorandom number (via MATLAB’s function “rand”) to each pixel;
- *salt and pepper noise* (with prescribed density), implemented using MATLAB’s “imnoise” function;
- *speckle noise* (with prescribed variance), implemented using MATLAB’s “imnoise” function.

Explanations of and values for the blur and noise parameters used in our tests are given in Section 4.

We now apply the following 4-step process to the signal  $f$ , where

$$f = N(\phi_b * z). \quad (2)$$

We denote the region of the finder pattern in the upper left corner by  $C_1$  and note that the part of the (clean) bar code which lies in this region is known a priori. Our method also works if any other known part of the bar code is used.

### 3.2 Step (i): Denoising via weighted TV flow

Our experiments show that if we perform denoising and kernel estimation at the same time, the results are much worse than when we dedicate separate steps to each procedure. Hence we first denoise the image using the weighted TV flow ([42, 43]),

$$\frac{\partial u}{\partial t} = \mu(t) \operatorname{div} \left( \frac{\alpha \nabla u}{|\nabla u|} \right) \quad (3)$$

with Neumann boundary conditions. Here the initial condition for  $u(x, t)$  is given by  $u(x, 0) := f$  and  $\alpha$  is a diffusion controlling function,

$$\alpha(x) := \frac{1}{\sqrt{1 + \frac{|(G_\sigma * \nabla f)(x)|^2}{\beta^2}}},$$

where  $G_\sigma$  is a normalized Gaussian function with mean zero and standard deviation  $\sigma$ .

The flow (3) is closely related to the standard total variation flow ([44, 45]), and can be obtained as a limiting case of hierarchical ( $BV_\alpha, L^2$ ) decomposition of  $f$  ([42]). Here, the  $BV_\alpha$  seminorm of  $u$  is defined as  $|u|_{BV_\alpha} := \int_\Omega \alpha |\nabla u|$ . In the hierarchical ( $BV_\alpha, L^2$ ) decomposition of  $f$ , finer scale components are removed from  $f$  successively, thus in the weighted TV flow,  $u(\cdot, t)$  becomes smoother as  $t$  increases ([42, 43]).

The weight function  $\alpha$  reduces the diffusion at prominent edges of the given QR image, i.e. at points  $x$  where the gradient  $|\nabla f|$  is high. The Gaussian smoothing avoids false characterization of noise as edges, and the value of  $\beta$  is chosen so

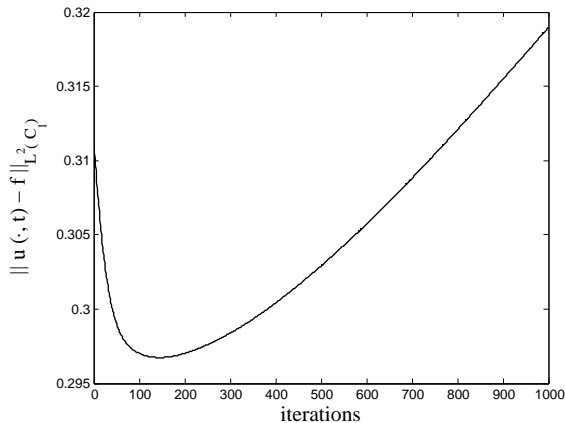


Figure 3: A typical run of the weighted TV flow, over which  $\|u(\cdot, t) - f\|_{L^2(C_1)}$  first decreases and then increases again.

that  $\alpha(x)$  is small at relevant edges in the image. The function  $\mu(t)$  in (3) is the monotonically increasing “speed” function. It can be shown (cf. [42]) that the speed of the flow is directly dependent on  $\mu(t)$ ; more precisely  $\|\frac{\partial u}{\partial t}\|_{\alpha^*} = \mu(t)$ , where  $\|\cdot\|_{\alpha^*}$  denotes the dual of the weighted  $BV_\alpha$  semi-norm, with respect to the  $L^2$  inner product.

We use homogeneous Neumann boundary conditions on the edges of the image (following [46, 47]), which are implemented in practice by extending the image outside its boundary with the same pixel values as those on the boundary.

The flow  $u(\cdot, t)$  reaches a constant value  $f_{avg}$  in finite time,  $T_f$  (cf. [45]). Hence, we need to decide upon the stopping time  $t_s$  for which  $u(\cdot, t_s)$  is a (near) optimally smoothed version of  $f$ . We take advantage of the fact that the upper left corner  $C_1$  is known a priori. We stop the flow at time  $t_s$  when the  $\|u(\cdot, t) - f\|_{L^2(C_1)}$  attains its minimum, and the function  $u_1 := u(\cdot, t_s)$  is taken as a denoised version of the QR code for further processing. This phenomenon is illustrated in Fig. 3. Thus, one of the advantages of using the weighted TV flow, over other minimization techniques, is that we do not need to change the

denoising parameters to get optimal results.

For the experiments in this paper, we choose  $\beta = 0.05$ , which corresponds to reduced regularization at relevant edges in the image  $f$ . The standard deviation of the Gaussian is empirically set to  $\sigma = 1$ . We expect that the denoised version is closer to the original image  $f$ , than to a coarse image obtained near  $T_f$ . Hence, the monotone increasing speed function  $\mu(t)$  is set to  $1.1^t$  to achieve higher accuracy near  $t = 0$ , cf. [43]. This is observed in Figure 3.

We also note that in earlier stages of experimentation we used a nonlocal TV approach for denoising (code from [48], based on the split Bregman technique described in [49]). Due to the edge-preserving property, the weighted TV flow technique described above gives better results with less rounded corners and so it is the one we have used to produce the results in this paper.

### 3.3 Step (ii): PSF estimation

To determine the blurring kernel we compare the known finder pattern in the upper left corner  $C_1$  of  $z$  with the same corner of  $u_1$ :

$$\phi_* = \operatorname{argmin}_{\phi} \int_{C_1} |\nabla \phi|^2 + \frac{\lambda_1}{2} \|\phi * z - u_1\|_{L^2(C_1)}^2.$$

Here  $\lambda_1 > 0$  is a parameter whose choice we will discuss in more detail in Section 3.6.

Note that this variational problem is strictly convex and hence possesses a unique minimizer which solves the Euler-Lagrange equation

$$-\Delta \phi_* + \lambda_1 (\phi_* * z - u_1) * z = 0.$$

Solving the equation in Fourier space, with the hat symbol denoting the Fourier transform, we find

$$\begin{aligned} -\hat{\Delta} \hat{\phi}_* + \lambda_1 (\hat{\phi}_* \hat{z} - \hat{u}_1) \hat{z} &= 0 \\ \Leftrightarrow (-\hat{\Delta} + \lambda_1 |\hat{z}|^2) \hat{\phi}_* - \lambda_1 \hat{u}_1 \hat{z} &= 0 \\ \Leftrightarrow \hat{\phi}_* &= (-\hat{\Delta} + \lambda_1 |\hat{z}|^2)^{-1} \lambda_1 \hat{u}_1 \hat{z}. \end{aligned}$$

We take the inverse Fourier transform to retrieve  $\phi_*$ . To ensure that the kernel is properly normalized, i.e.  $\int \phi_* = 1$ , we normalize the input signals  $u_1$  and  $z$  to unit mass before applying the algorithm.

To reduce the influence of boundary effects in the above procedure, we impose periodic boundary conditions, by extending (the corners of) both  $z$  and  $u_1$  with their mirror images on all sides, and extracting the center image, corresponding to the original image (corner) size, from the result after minimization.

The output of the algorithm is of the same size as  $C_1$ , even though the actual kernel is smaller. To make up for this we reduce the size of the kernel afterwards by manually cutting it down to a smaller size. We determine this smaller size semi-automatically by constructing a collection  $\{\phi_1, \phi_2 \dots, \phi_n\}$  of kernels of different sizes by reducing  $\phi_*$  and selecting the  $\phi_i$  for which  $\|\phi_i * z - u_1\|_{L^2(C_1)}^2$  is minimized. This comparison is fairly quick and in practice we compare kernels of many or all sizes up to the full size of the original output. It is important to normalize the reduced kernel again to unit mass. This is the kernel we will denote by  $\phi_*$  in the following.

### 3.4 Step (iii): Deblurring (Deconvolution)

With the minimizing kernel  $\phi_*$ , we then proceed to deblur the denoised signal  $u_1$  via the variational problem

$$u_2 = \operatorname{argmin}_u \int |u_x| + |u_y| + \frac{\lambda_2}{2} \|\phi_* * u - u_1\|_{L^2}^2.$$

We will discuss the choice of the parameter  $\lambda_2 > 0$  in Section 3.6.

This minimization problem is solved via the split Bregman iteration method [41, ATV\_NB\_Deconvolution], described previously in Section 2. This algorithm uses an internal fidelity parameter for the split variables, whose value we set to 100. We use 2 internal Bregman iterations.

We again impose periodic boundary conditions, by extending  $u$  and  $u_1$  with mirror images, and extracting the center image, corresponding to the original image size, from the result.

### 3.5 Step (iv): Thresholding

Finally we threshold the result based on the gray value per pixel to get a binary image  $u_3$ . We determine the threshold value empirically by trying out a set of different values and pick the one that minimizes the comparison with the clean corner  $\|u_3 - z\|_{L^2(C_1)}^2$ .

Instead of thresholding per pixel, we also experimented with thresholding the end result based on the average gray value per block of pixels of size X-dimension by X-dimension, again using an empirically optimized threshold value as above. Our tests show that thresholding per pixel works a lot better than thresholding per block, despite the output of the latter often being more ‘bar code like’. Figure 4 shows an example of a bar code for which the blurred and noisy version, nor the cleaned version when thresholded per block can be read by *ZBar*, but the cleaned version thresholded per pixel can be read. This is a common occurrence. Hence, in the remainder of this paper we will only consider thresholding per pixel.

In the final output we add back the known parts of the QR bar code, i.e., the *required patterns* of Figure 2.

### 3.6 Fidelity parameter estimation

Good choices of the fidelity parameters are crucial to the success of the algorithm. To this end, we again exploit the known structures in the QR code. In the original Rudin-Osher-Fatemi model [35], if the data is noisy, but not blurred, the fidelity parameter  $\lambda$  should be inversely proportional to the variance of the noise [11, Section 4.5.4]. Hence we set  $\lambda_2 = 1/\sigma_2^2$ , where  $\sigma_2^2$  is the variance of  $(\phi_* * z - u_1)|_{C_1}$ . We cannot use the same heuristic to choose  $\lambda_1$ , because we do not know exactly the ‘clean’ true kernel  $\phi_b$ . There-

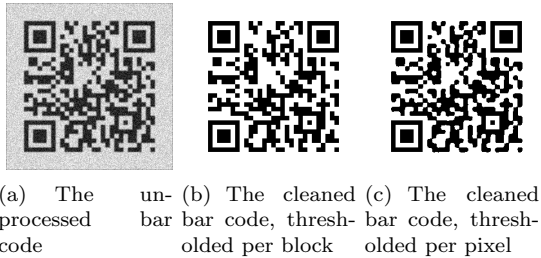


Figure 4: Code 1 with Gaussian blur (kernel size 3, standard deviation 3) and Gaussian noise (mean 0.3, variance 0.2). Neither the blurry and noisy bar code, nor the cleaned code that is thresholded per block, can be read by *ZBar*. The cleaned code that is thresholded per pixel can be read.

fore  $\lambda_1$  is a free parameter that needs to be input when the algorithm is run. In our experiments we use  $\lambda_1 = 10000$ .

The heuristic for choosing the fidelity parameter  $\lambda_2$  is based on the assumption that the signal  $u_1$ , which is to be cleaned, is not blurred. Hence the expectation, which was borne out by some testing, is that this automatic choice of  $\lambda_2$  works better for small blurring kernels, than for large ones. For the latter we could possibly improve the results by manually choosing  $\lambda_2$  (by trial and error), but the results reported in this paper are all for automatically chosen  $\lambda_2$ . If much of the noise is already removed due to a large blurring kernel, the automatic algorithm overestimates the variance of the noise and hence underestimates  $\lambda_2$ .

## 4 Results

As described in Section 3, we tested our algorithm on a selection of blurred and noisy bar codes, with either Gaussian blur or motion blur, and four types of noise (additive random, Gaussian, speckle, and salt and pepper). We then compared the performance of the *ZBar* software on this catalogue, before and after cleaning up

the bar codes with our algorithm. All the results discussed in this section pertain to the case in which we use the weighted TV flow (instead of a nonlocal TV approach) in step (i) of our algorithm and we threshold per pixel (not by block) in step (iv).

### 4.1 Choice of noise and blurring parameters

Our original clean binary images are normalized to take values in  $\{0, 1\}$ .

To construct a rotationally symmetric, normalized, Gaussian blur kernel with MATLAB’s function “*fspecial*”, we need to specify two free parameters: the size (i.e. the number of rows) of the square blurring kernel matrix and the standard deviation of the Gaussian. We vary the former over the values in  $\{3, 7, 11, 15, 19\}$ , and the latter over the values in  $\{3, 7, 11\}$ .

To construct a motion blur matrix with “*fspecial*”, we need to specify the angle of the motion and the length of the linear motion. For all our experiments we fix the former at 30 degrees and vary the latter over  $\{3, 7, 11, 15, 19\}$  pixels.

Because our Gaussian blur kernels have one more free parameter than our motion blur kernels, we use a larger range of noise parameters for the latter case.

To create additive noise, we add  $c_{add}$  times a matrix of i.i.d. pseudorandom numbers (drawn from the standard normal distribution) to the image. In case of Gaussian blur we use  $c_{add} = 0.05$ , for the motion blur case we vary  $c_{add}$  over  $\{0, 0.05, 0.1, \dots, 0.4, 0.45, 0.5\}$ .

To construct Gaussian noise, we need to specify its mean and standard deviation. In the Gaussian blur case, we fix this mean at 0.3 and this variance at 0.2. In the motion blur case we fix the mean at 0.7 and vary the variance over  $\{0, 0.1, 0.2, \dots, 0.8, 0.9, 1\}$ .

Salt and pepper noise requires the input of one parameter: its density. In the Gaussian blur case, we fix the density at 0.2; in the motion blur case we vary it over  $\{0, 0.1, 0.2, \dots, 0.8, 0.9, 1\}$ .

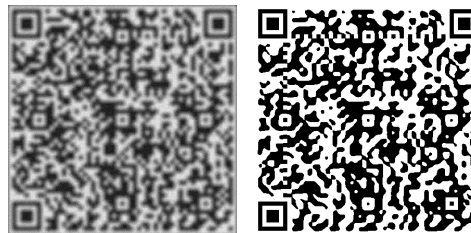
Finally, to produce speckle noise we have to

specify its variance. In the Gaussian blur case, we fix this at 0.4; in the motion blur case we vary the variance over  $\{0, 0.1, 0.2, \dots, 0.8, 0.9, 1\}$ .

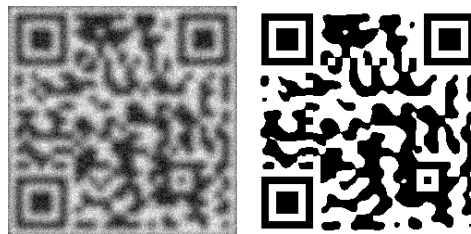
Each of the resulting blurry and noisy bar codes is again normalized, such that each pixel has a gray value between 0 and 1.

## 4.2 Some examples of cleaned up bar codes

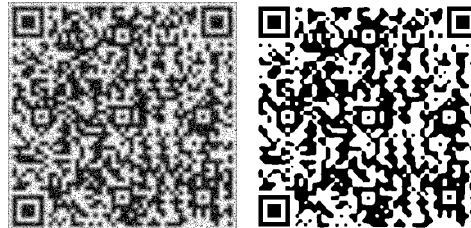
Figures 5 and 6 show examples for our blind deblurring and denoising process. Figure 5 shows QR bar codes with Gaussian blur and various types of noise, together with their cleaned versions that were output by our algorithm. In all these cases the software *ZBar* was not able to read the blurred and noisy bar code, but was able to read the output of our algorithm. Figure 6 shows similar examples for QR bar codes with motion blur. We want to stress that we do not use subjective aesthetic pleasantness as the arbiter of whether our reconstruction is good or not, but we test if the output can be read by the *ZBar* bar code reading software.



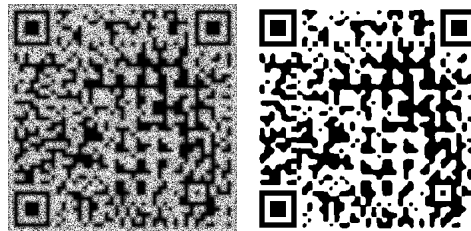
(a) Code 7 with Gaussian blur (size 11, standard deviation 11) and additive noise (level 0.05) (b) The code from Figure 5(a) cleaned



(c) Code 9 with Gaussian blur (size 11, standard deviation 11) and Gaussian noise (mean 0.3, variance 0.2) (d) The code from Figure 5(c) cleaned



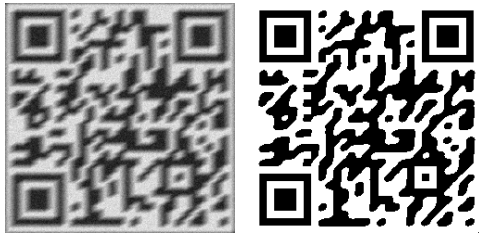
(e) Code 10 with Gaussian blur (size 7, standard deviation 11) and salt and pepper noise (density 0.2) (f) The code from Figure 5(e) cleaned



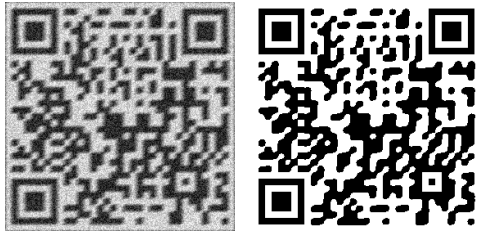
(g) Code 5 with Gaussian blur (size 7, standard deviation 7) and speckle noise (variance 0.6) (h) The code from Figure 5(g) cleaned

Figure 5: Some examples of QR bar codes with Gaussian blur and various types of noise, and the corresponding cleaned output of our algorithm which can be read by the *ZBar* software.

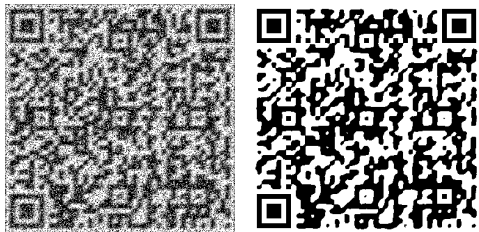




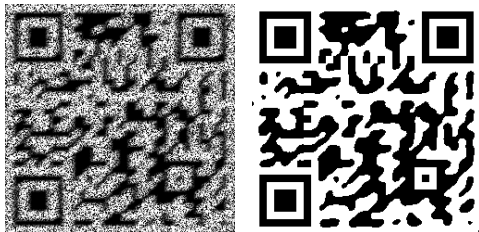
(a) Code 2 with motion blur (length 11, angle 30) and additive noise (level 0.05) (b) The code from Figure 6(a) cleaned



(c) Code 3 with motion blur (length 7, angle 30) and Gaussian noise (mean 0.7, variance 0.3) (d) The code from Figure 6(c) cleaned



(e) Code 4 with motion blur (length 7, angle 30) and salt and pepper noise (density 0.4) (f) The code from Figure 6(e) cleaned



(g) Code 9 with motion blur (length 7, angle 30) and speckle noise (variance 0.6) (h) The code from Figure 6(g) cleaned

### 4.3 Results of our algorithm

To check that our results are not heavily influenced by the specifics of the original clean bar code or by the particular realization of the stochastic noise, we run our experiments on ten different bar codes (three are shown in Figure 7), per code averaging the results (0 for “not readable by *ZBar*” and 1 for “readable by *ZBar*”) over ten realizations of the same stochastic noise. These tests lead to the sixteen ‘phase diagrams’ in Figures 8–15. Note that each diagram shows the average results over ten runs for one particular choice out of the ten codes. Dark red indicates that the *ZBar* software is able to read the bar code (either the blurry/noisy one or the cleaned output of our algorithm) in all ten runs, and dark blue indicates that *ZBar* cannot read any of the ten runs. Note that the bar codes displayed in Figures 5 and 6 are chosen from parts of the phase diagrams where the output is readable in all runs. While each phase diagram only pertains to one of the ten codes we used, our results showed that the results were quite robust with respect to variation in the codes used.

Before we delve into the specific outcomes, note one general trend for motion blur: in the absence of noise and at high blurring (length 15), the cleaned bar codes are not readable, while the uncleaned ones are. Running our algorithm on the noiseless images without including denoising Step (i) (Section 3.2) does not fix this issue. In the case of Gaussian blur this issue does typically not occur. We are rather puzzled as to the cause of (and remedy for) this behavior. In the presence of even the slightest noise this issue disappears. Noise generally renders the uncleaned bar codes completely unreadable (with a minor exception for low level additive noise in Figure 9(a)). Those are the situations in which our algorithm delivers.

#### 4.3.1 Additive random noise

From Figure 8, we see that *ZBar* performs very badly in the presence of additive noise even at low noise additive noise level 0.05. The bar code

Figure 6: Some examples of QR bar codes with motion blur and various types of noise, and the corresponding cleaned output of our algorithm which can be read by the *ZBar* software.



Figure 7: Some of the clean bar codes used in the experiments

Kernel size	Standard deviation	Unprocessed	Cleaned
3	3	0	0.72
3	7	0	0.78
3	11	0	0.8
7	3	0	1
7	7	0	0.99
7	11	0	1
11	3	0	0.96
11	7	0	0.69
11	11	0	0.64
15	3	0	0.89
15	7	0	0
15	11	0	0
19	3	0	0.92
19	7	0	0
19	11	0	0

is only readable for small blurring kernel. The cleaned codes however are consistently readable for quite a large range of blur kernel size and standard deviation.

In the motion blur case, Figure 9, there is a slight, but noticeable improvement in readability for low level additive noise at larger size blur kernels. As we will see below, however, in the presence of motion blur, additive noise is clearly the type of noise our algorithm has the most difficulties with.

### 4.3.2 Gaussian noise

In Figure 10 we see that bar codes with Gaussian blur and noise are completely unreadable by *ZBar* at the noise level we used. Our algorithm gives a massive improvement, turning the code readable for all but the highest blur kernel size/standard deviation combinations.

As shown in Figure 11 a similar situation arises for motion blur. In the presence of any Gaussian noise, the motion blurred bar code is unreadable. Our algorithm consistently makes low noise codes readable, while also leading to readability for nontrivial percentages of high level codes.

In the Tables 1 and 2 we explicitly list some results for the Gaussian noise case.

Table 1 shows the fraction of unprocessed and cleaned codes that was readable by *ZBar*, when the original code was degraded with Gaussian blur (with the kernel sizes and standard deviations as listed in the table) and Gaussian noise (mean 0.3 and variance 0.2). Note that the read-

Table 1: Readability of bar codes with Gaussian blur (kernel sizes and standard deviations listed) and Gaussian noise (mean 0.3, variance 0.2). The columns “Unprocessed” and “Cleaned” show the fraction of all codes (10 different codes, 10 different noise instantiations for each code) that were readable by *ZBar*.

ability in the last two columns is given as the fraction of all codes (i.e. all ten versions of each of the ten codes used, thus one hundred codes in total) at those particular blur levels that were readable by *ZBar*. Note the difference with the diagrams in Figure 10, which only show the average results over the ten versions of the specific Code 9.

We note that the results in Table 1 are very similar to those in Figure 10, suggesting that the exact form of the original clean bar code does not have a large influence on our algorithm’s results. Also note that our algorithm improves the readability of the unprocessed bar codes greatly.

Table 2 should be interpreted in a similar way to Table 1 and shows the case for motion blur (with the blurring lengths as listed in the table) and Gaussian noise (with fixed mean 0.7 and variances as listed in the table). Again we see a high similarity with the single-code results in the diagram of Figure 11 and an overall significant increase in readability after applying our algorithm to the unprocessed bar code.

Length	Variance	Unprocessed	Cleaned
3	0	1	1
3	1	0	0.99
3	2	0	0.79
3	3	0	0.6
3	4	0	0.32
3	5	0	0.32
3	6	0	0.26
3	7	0	0.31
3	8	0	0.24
3	9	0	0.31
3	10	0	0.37
7	0	1	1
7	1	0	0.98
7	2	0	0.99
7	3	0	0.93
7	4	0	0.8
7	5	0	0.74
7	6	0	0.62
7	7	0	0.71
7	8	0	0.67
7	9	0	0.58
7	10	0	0.49
11	0	1	1
11	1	0	0.93
11	2	0	0.89
11	3	0	0.76
11	4	0	0.59
11	5	0	0.75
11	6	0	0.58
11	7	0	0.46
11	8	0	0.44
11	9	0	0.47
11	10	0	0.39

Table 2: Readability of bar codes with Motion blur (blur lengths listed) and Gaussian noise (mean 0.7, variances listed). The columns “Unprocessed” and “Cleaned” show the fraction of all codes (10 different codes, 10 different noise instantiations for each code) that were readable by *ZBar*. The table does not show the results for blur lengths 15 and 19. Readability of the cleaned codes at these values is near or equal to zero.

#### 4.3.3 Salt and pepper noise

In Figures 12 and 13 we see that the case for salt and pepper noise is very similar to that of Gaussian noise, but for Gaussian blur and motion blur. Our algorithm seems to have a slightly

harder time for large Gaussian blur kernels in the presence of salt and pepper noise, than was the case for Gaussian noise. It also does not show the same kind of partial results for high noise levels in the presence of motion blur, although it performs more consistently at medium salt and pepper noise levels, than it did at medium Gaussian noise levels.

#### 4.3.4 Speckle noise

The case of speckle noise is quite similar to those of Gaussian noise and salt and pepper noise before, as we see in Figures 14 and 15. We note however that the case of large Gaussian blur kernels is a difficult one now, with very low readability, while on the other hand the improvement in the readability of the motion blurred codes is consistently high and better than we have seen for any of the other types of noise.

## 5 Final Comments

We have presented and tested a purely regularization based algorithm for blind deblurring and denoising of QR bar codes. The strengths of our method is that it is ansatz-free with respect to the structure of the PSF and the noise. In particular, it can deal with motion blurring. While we have not tried to optimize for speed here, there is currently much research into fast implementations of Bregman iteration, and hence the speed of these regularization methods continues to improve. One inherent weakness of our method is that Step 2 (PSF estimation) imposes restrictions on the size (standard deviation) of the unknown blurring kernel, with successful implementation limited to roughly the order of the module width.

Given that most articles in image processing which present a new method end with comparisons with known methods, a few comments are in order. First off, one of the benefits of working with QR bar codes is that we do not need to, or want to, assess our results with the “eye-ball

norm”, but rather with bar code reading software such as the open source *ZBar*. While we know of no other method specifically designed for blind deblurring and denoising of QR codes, the closest method is that of [34] for matrix 2D codes. That method is based upon a Gaussian ansatz for noise and blurring, but also exploits a finder pattern, which in that case is an L-shaped corner. While they use a different reading software *ClearImage* [50], it would be interesting to adapt their method to QR codes, and compare their results with ours for Gaussian blurring and noise. We have not included such a comparison in the present paper, because we do not have access to either the same hardware (printer, camera) or software used in [34]. Since the results in that paper depend heavily on these factors, any comparison produced with different tools would be misleading.

## Acknowledgments

A significant part of the first and third authors’ work was performed while they were at the Department of Mathematics at UCLA. The work of RC was partially supported by an NSERC (Canada) Discovery Grant.

## References

- [1] “ZBar bar code reader,” <http://zbar.sourceforge.net/>
- [2] R. Palmer, *The Bar Code Book: A Comprehensive Guide to Reading, Printing, Specifying, Evaluating, and Using Bar Code and Other Machine-Readable Symbols*, fifth edition (Trafford Publishing, 2007).
- [3] “QR Stuff,” <http://www.qrstuff.com>
- [4] Wikipedia, “QR Code,” [http://en.wikipedia.org/wiki/QR\\_code](http://en.wikipedia.org/wiki/QR_code)
- [5] W. Turin, R.A. Boie, “Bar code recovery via the EM algorithm,” *IEEE Trans. Signal Process.* **46**(2), 354–363 (1998).
- [6] H. Kato, K.T. Tan, “Pervasive 2D barcodes for camera phone applications,” *IEEE Pervasive Comput.* **6**(4), 76–85 (2007).
- [7] O. Eisaku, H. Hiroshi, A.H. Lim, “Barcode readers using the camera device in mobile phones,” in *Proc. 2004 Internat. Conf. on Cyber worlds, Tokyo, Japan* (2004), pp. 260–265.
- [8] J.T. Thielemann, H. Schumann-Olsen, H. Schulerud, and T. Kirkhus, “Handheld PC with camera used for reading information dense barcodes,” in *Proc. IEEE Int. Conf. on Computer Vision and Pattern Recognition, Demonstration Program, Washington, DC* (2004).
- [9] C.-H. Chu, D.-N. Yang, and M.-S. Chen, “Image stabilization for 2d barcode in handheld devices,” in *Proceedings of the 15th International Conference on Multimedia 2007, Augsburg, Germany, September 24-29, 2007*, R. Lienhart, A. R. Prasad, A. Hanjalic, S. Choi, B. P. Bailey, and N. Sebe, eds., (ACM, 2007), pp. 697–706.
- [10] H. Yang, C. Alex, and X. Jiang, “Barization of low-quality barcode images captured by mobile phones using local window of adaptive location and size,” *IEEE Trans. Image Process.* **21**(1), 418–425 (2012).
- [11] T. F. Chan and J. Shen, *Image Processing and Analysis: Variational, PDE, Wavelet, and Stochastic Methods* (Society for Industrial and Applied Mathematics, 2005).
- [12] Y. You and M. Kaveh, “A regularization approach to joint blur identification and image restoration,” *IEEE Trans. Image Process.* **5**, 416–428 (1996).
- [13] T. F. Chan and C.K. Wong, “Total variations blind deconvolution,” *IEEE Trans. Image Process.* **7**, 370–375 (1998).
- [14] R. Molina, J. Mateos, and A. K. Katsaggelos, “Blind deconvolution using a variational approach to parameter, image, and

- blur estimation,” *IEEE Trans. Image Process.* **15**(12), 3715–3727 (2006).
- [15] L. Bar, B. Berkels, M. Rumpf, and G. Sapiro, “A variational framework for simultaneous motion estimation and restoration of motion-blurred video,” in *Proc. ICCV* (2007), pp. 1–8.
- [16] P. D. Romero and V. F. Candela, “Blind deconvolution models regularized by fractional powers of the Laplacian,” *J. Math. Imag. Vis.* **32**(2), 181–191 (2008).
- [17] L. He, A. Marquina, and S. Osher, “Blind deconvolution using TV regularization and Bregman iteration,” *Int. J. Imag. Syst. Technol.* **15**(1), 74–83 (2005).
- [18] Q. Shan, J. Jia, and A. Agarwala, “High-quality motion deblurring from a single image,” in *Proc. SIGGRAPH* (2008), 1–10.
- [19] H. Takeda and P. Milanfar. “Removing Motion Blur with Space-Time Processing,” *IEEE Trans Image Process.* **10**, 2990–3000 (2011).
- [20] M. M. Bronstein, A. M. Bronstein, M. Zibulevsky, and Y. Y. Zeevi, “Blind deconvolution of images using optimal sparse representations,” *IEEE Trans. Image Process.* **14**(6), 726–736 (2005).
- [21] D. G. Tzikas, A. C. Likas, and N. P. Galasanos, “Variational Bayesian sparse kernel-based blind image deconvolution with student’s t-priors,” *IEEE Trans. Image Process.* **18**(4), 753–764 (2009).
- [22] J.-F. Cai, S. Osher, and Z. Shen, “Linearized Bregman iterations for frame-based image deblurring,” *SIAM J. Imag. Sci.* **2**(1), 226–252 (2009).
- [23] J.-F. Cai, H. Ji, C. Liu, and Z. Shen, “Blind motion deblurring from a single image using sparse approximation,” in *Proc. CVPR* (2009), pp. 104–111.
- [24] J.-F. Cai, H. Ji, C. Liu, and Z. Shen, “Framelet-based blind motion deblurring from a single image,” *IEEE Trans. Image Process.* **21**(2), 562–572 (2012).
- [25] E. Joseph, T. Pavlidis, “Bar code waveform recognition using peak locations,” *IEEE Trans. Pattern Anal. Machine Intell.* **16**(6), 630–640 (1994).
- [26] S. Kresic-Juric, “Edge detection in bar code signals corrupted by integrated time-varying speckle,” *Pattern Recognition* **38**(12), 2483–2493 (2005).
- [27] S. Kresic-Juric, D. Madej, F. Santosa, “Applications of hidden Markov models in bar code decoding,” *Pattern Recognition Lett.* **27**(14), 1665–1672 (2006).
- [28] J. Kim, H. Lee, “Joint nonuniform illumination estimation and deblurring for bar code signals,” *Opt. Express* **15**(22), 14817–14837 (2007).
- [29] S. Esedoglu, “Blind deconvolution of bar code signals,” *Inverse Problems* **20**, 121–135 (2004).
- [30] R. Choksi and Y. van Gennip, “Deblurring of One Dimensional Bar Codes via Total Variation Energy Minimization,” *SIAM J. on Imaging Sciences* **3**(4), 735–764 (2010).
- [31] M.A. Iwen, F. Santosa, R. Ward, “A symbol-based algorithm for decoding bar codes,” *SIAM J. Imaging Sci.* **6**(1), 56–77 (2013).
- [32] D. Parikh and G. Jancke, “Localization and segmentation of a 2D high capacity color barcode,” in *Proc. 2008 IEEE Workshop on Applications of Computer Vision* (2008), pp. 1–6.
- [33] W. Xu and S. McCloskey, “2D barcode localization and motion deblurring using a flutter shutter camera,” in *2011 IEEE Workshop on Applications of Computer Vision (WACV)*, (2011), pp. 159–165.

- [34] N. Liu, X. Zheng, H. Sun, X. Tan, “Two-dimensional bar code out-of-focus deblurring via the Increment Constrained Least Squares filter,” *Pattern Recognition Letters* **34**, 124–130 (2013).
- [35] L. I. Rudin, S. Osher, and E. Fatemi, “Non-linear total variation based noise removal algorithms,” *Physica D* **60**, 259–268 (1992).
- [36] S. Esedoglu and S. Osher, “Decomposition of images by the anisotropic Rudin-Osher-Fatemi model,” *Comm. Pure Appl. Math.* **57**, 1609–1626 (2004).
- [37] R. Choksi, Y. van Gennip, and A. Oberman, “Anisotropic Total Variation Regularized  $L^1$ -Approximation and Denoising/Deblurring of 2D Bar codes,” *Inverse Problems and Imaging* **5**(3), 591–617 (2011).
- [38] G. Gilboa and S. Osher, “Nonlocal operators with applications to image processing,” *Multiscale Model. Simul.* **7**, 1005–1028 (2008).
- [39] W. Yin, S. Osher, J. Darbon, and D. Goldfarb. “Bregman Iterative Algorithms for Compressed Sensing and Related Problems,” *SIAM Journal on Imaging Sciences* **1**(1), 143–168 (2008)
- [40] T. Goldstein and S. Osher, “The split Bregman method for  $L^1$  regularized problems,” *SIAM Journal on Imaging Sciences* **2**(2), 323–343 (2009).
- [41] J. Gilles, “The Bregman Cookbook,” <http://www.mathworks.com/matlabcentral/fileexchange/35462-bregman-cookbook>
- [42] P. Athavale, R. Xu, P. Radau, A. Nachman, and G. Wright, “Multiscale TV flow with applications to fast denoising and registration,” *SPIE Medical Imaging, International Society for Optics and Photonics*, 86692K1–86692K7 (2013).
- [43] R. Xu and P. Athavale “Multiscale Registration of Realtime and Prior MRI Data for Image Guided Cardiac Interventions,” *IEEE Transactions on Biomedical Engineering*, Advance online publication, doi: 10.1109/TBME.2014.2324998 (2014).
- [44] F. Andreu, C. Ballester, V. Caselles, and J. Mazón, “Minimizing total variation flow,” *Differential and integral equations*, **14**(3), 321–360 (2001).
- [45] F. Andreu and V. Caselles and J. Diaz and J. Mazón, “Some qualitative properties for the total variational flow,” *Journal of functional analysis*, **188**, 516–547 (2002).
- [46] E. Tadmor, S. Nezzar, and L. Vese. “A Multiscale Image Representation Using Hierarchical (BV,L2) Decompositions,” *Multiscale Modeling & Simulation* **4**(2), 554–579 (2004).
- [47] E. Tadmor, S. Nezzar, and L. Vese. “Multiscale hierarchical decomposition of images with applications to deblurring, denoising, and segmentation,” *Communications in Mathematical Sciences* **6**(2), 281–307 (2008).
- [48] Y. Mao and Jérôme Gilles, “Non rigid geometric distortions correction - Application to Atmospheric Turbulence Stabilization,” *Journal of Inverse Problems and Imaging* **6**(3), 531–546 (2012).
- [49] X. Zhang and M. Burger and X. Bresson and S. Osher, “Bregmanized Nonlocal Regularization for Deconvolution and Sparse Reconstruction,” *SIAM Journal on Imaging Sciences*, **3**(3), 253–276 (2010).
- [50] “ClearImage Free Online Barcode Reader / Decoder,” <http://online-barcode-reader.inliteresearch.com/>

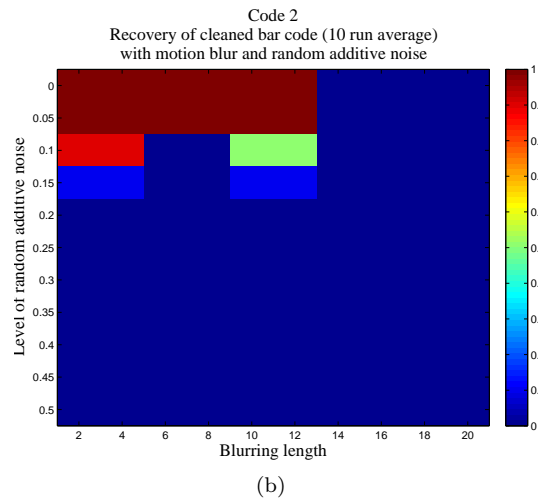
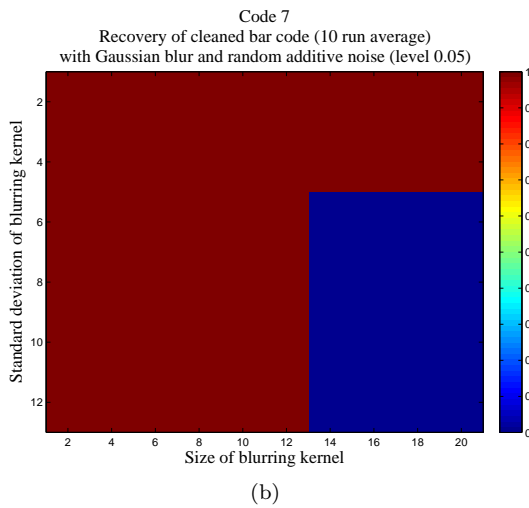
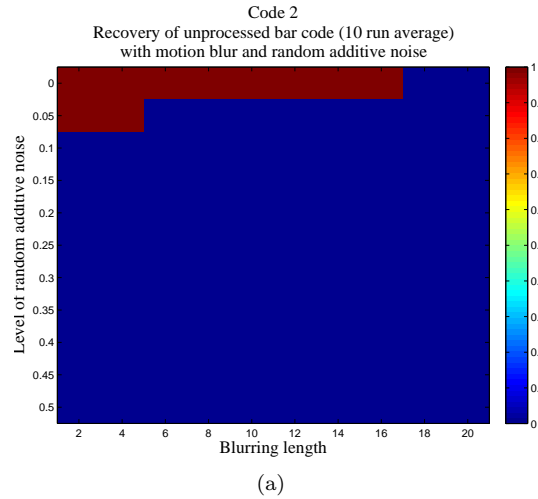
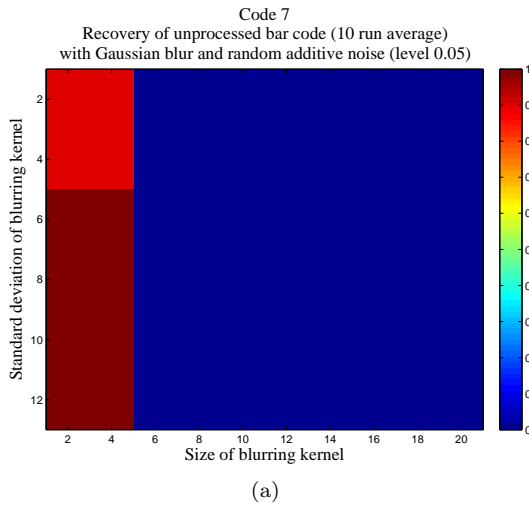
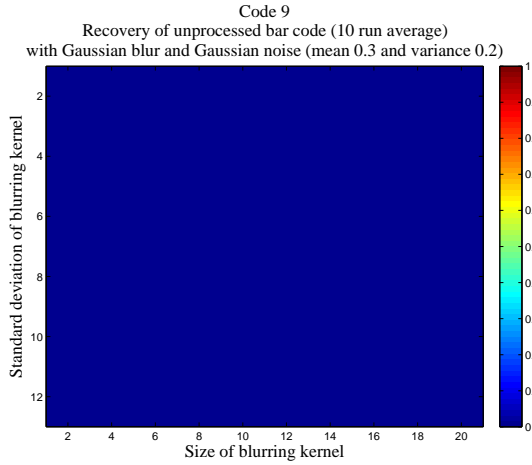
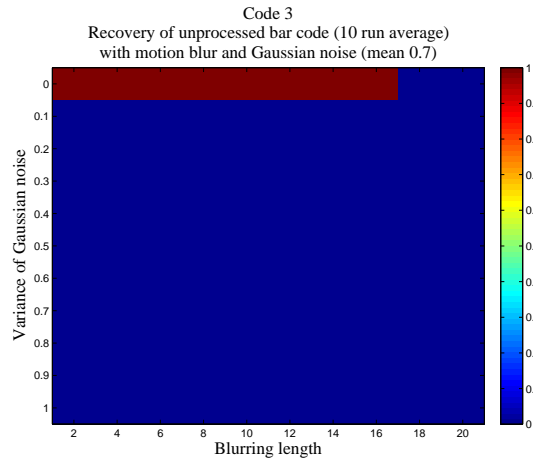


Figure 8: Bar code readability of the unprocessed and cleaned Code 7, for various sizes and standard deviations of the Gaussian blur kernel, with additive noise (level 0.05). The color scale indicates the fraction of ten runs with different noise realizations which lead to a bar code readable by the *ZBar* software

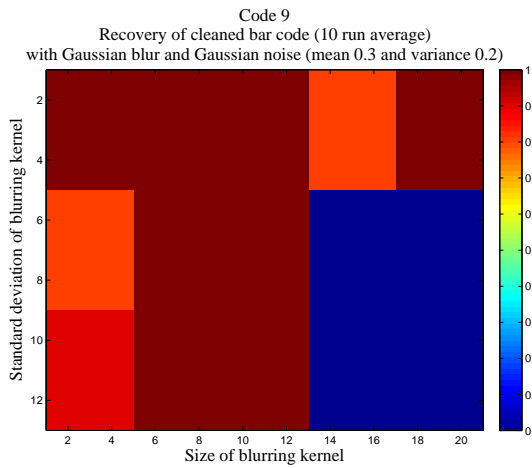
Figure 9: Readability for Code 2 from Figure 7(a), for various blurring lengths and various values of the additive noise level.



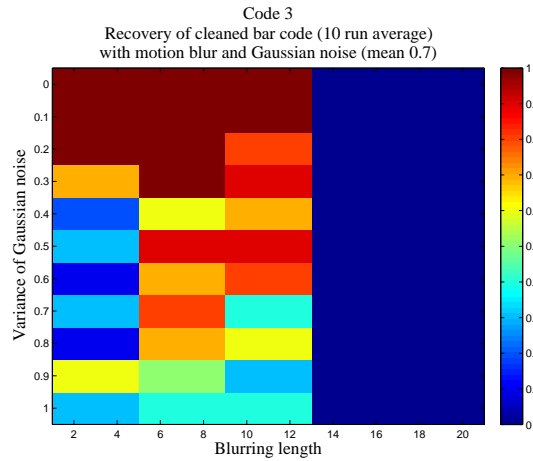
(a)



(a)



(b)



(b)

Figure 10: Readability for Code 9 from Figure 7(b), for various sizes and standard deviations of the Gaussian blur kernel, with Gaussian noise (mean 0.3, variance 0.2).

Figure 11: Readability of Code 3, for various blurring lengths and various values of the Gaussian noise variance (with mean 0.7).



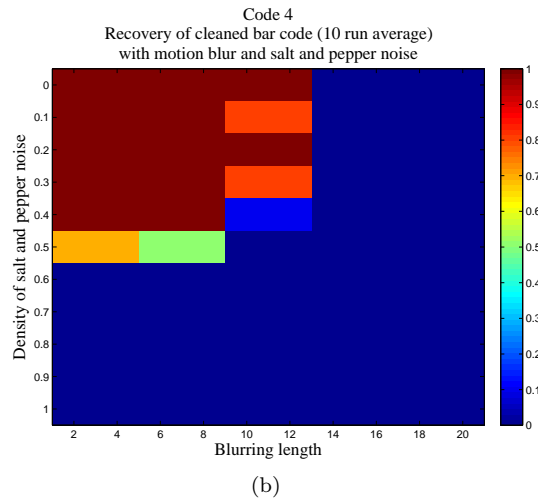
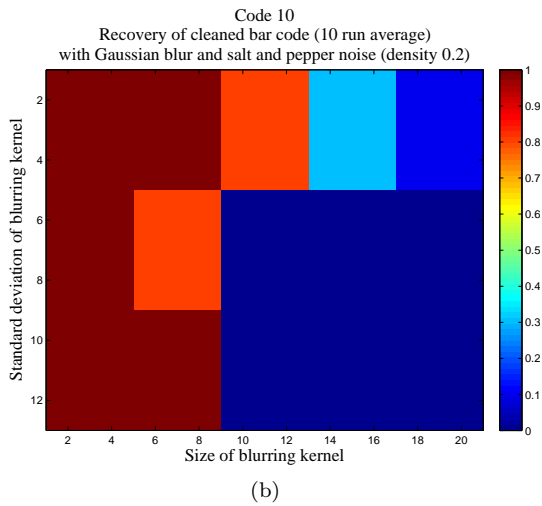
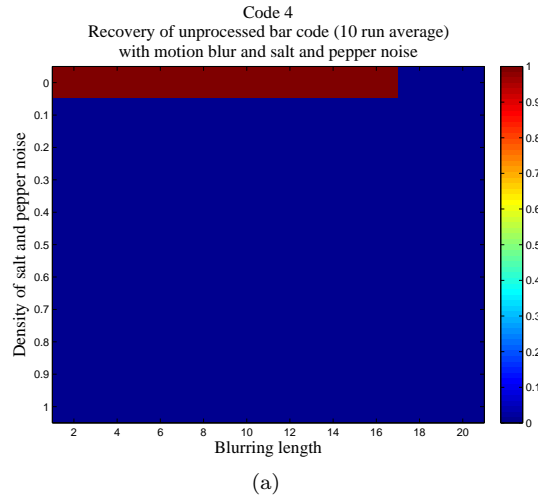
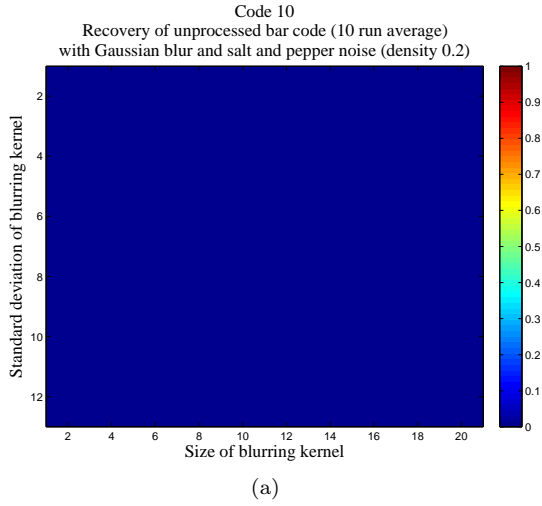
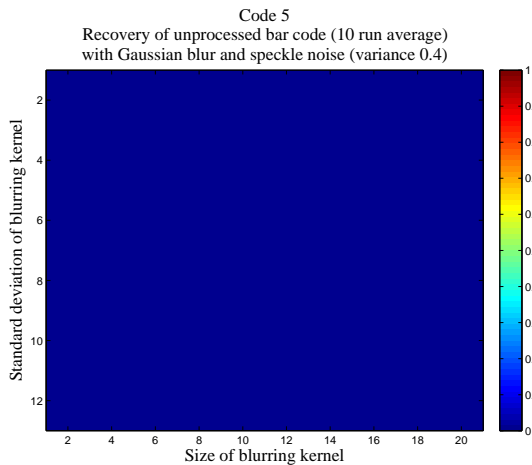
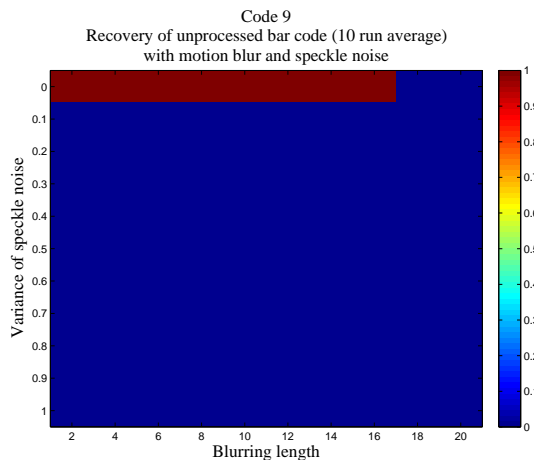


Figure 12: Readability of Code 10 from Figure 7(c), for various sizes and standard deviations of the Gaussian blur kernel, with salt and pepper noise (density 0.2).

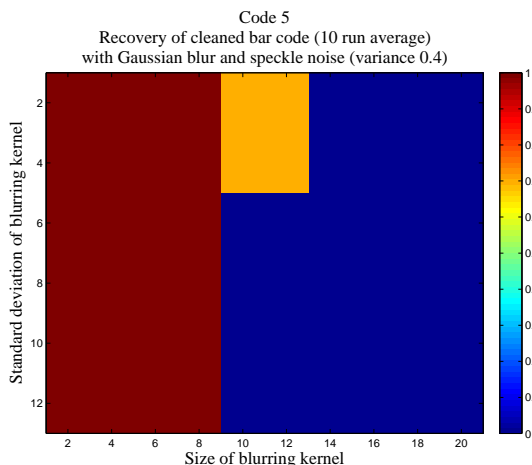
Figure 13: Readability of Code 4, for various blurring lengths and various values of the salt and pepper noise density.



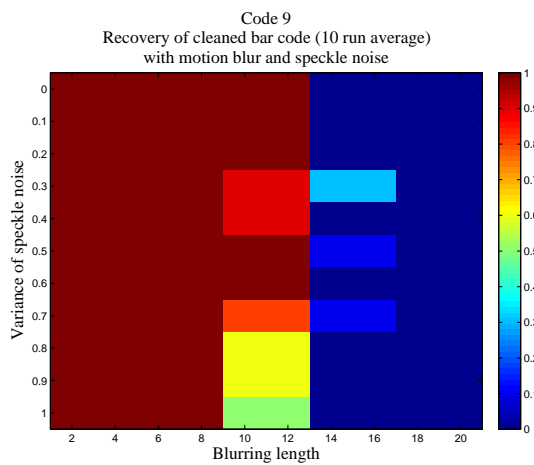
(a)



(a)



(b)



(b)

Figure 14: Readability of Code 5, for various sizes and standard deviations of the Gaussian blur kernel, with speckle noise (variance 0.4).

Figure 15: Readability of Code 9 from Figure 7(b), for various blurring lengths and various values of the speckle noise variance.